2.1 DEVELOPMENT OF ODS FeCrAl FOR FUSION REACTOR APPLICATIONS – D. T. Hoelzer, K. A. Unocic, S. Dryepondt and B. A. Pint (Oak Ridge National Laboratory, USA)

OBJECTIVE

The dual coolant lead-lithium (DCLL) blanket concept requires improved Pb-Li compatibility with ferritic steels in order to demonstrate viable blanket operation in a DEMO-type fusion reactor. The goal of this work is to develop an oxide dispersion strengthened (ODS) alloy with improved compatibility with Pb-Li and excellent mechanical properties. The current focus is characterizing the first batch of ODS Fe-12Cr-5Al.

SUMMARY

Three experimental ODS FeCrAl heats of composition Fe-12Cr-5Al were prepared by mechanical alloying with additions of Y_2O_3, Y_2O_3 + ZrO_2 and Y_2O_3 + HfO_2. The as-extruded microstructure showed smaller grain size with the co-additions of ZrO_2 or HfO_2 and high concentrations of nano-size (<5 nm diameter) oxide particles within the grains. In the alloy with Y_2O_3 + HfO_2, either a bimodal or trimodal particle size distribution was observed. Tensile testing was performed at 25° up to 800°C and the higher oxide contents with ZrO_2 or HfO_2 resulted in higher yield and ultimate strengths but lower ductility compared to the alloy with only Y_2O_3.

PROGRESS AND STATUS

Introduction

The DCLL blanket concept (Pb-Li and He coolants) is the leading U.S. design for a test blanket module (TBM) for ITER and for a DEMO-type fusion reactor.[1] With reduced activation ferritic-martensitic (FM) steel as the structural material, the DCLL is limited to ~475°C metal temperature because Fe and Cr readily dissolve in Pb-Li above 500°C and Eurofer 97 plugged a Pb-Li loop at 550°C.[2-3] For a higher temperature blanket for DEMO, structural materials with enhanced creep and compatibility are needed. ODS FeCrAl alloys are one possibility to meet this objective and considerable research on ODS FeCr alloys has shown an excellent combination of creep strength and radiation resistance.[4-7] However, these ODS FeCr alloys do not have adequate compatibility with Pb-based coolants, such as Pb-Bi eutectic (LBE) [8-11]. With the addition of Al, isothermal compatibility tests have shown low mass losses at up to 800°C.[12] Therefore, a materials development effort is underway, specific to this application. ODS FeCrAl was commercialized in the 1970's for its high temperature (>1000°C) creep and oxidation resistance [13] and other research groups are currently investigating new FeCrAl alloy compositions for fission and fusion applications with liquid metals.[14-16]

Previously, initial work was presented to identify composition factors such as the stability of ternary oxides and the Pb-Li compatibility of cast model FeCrAl alloys.[17,18] While previous studies found good Pb-Li compatibility for Fe-20wt.%Cr-5.5Al,[12] there is concern about thermal ageing embrittlement and the formation of α' during irradiation due to the high Cr content [19]. Thus, the initial alloy fabrication focused on a base alloy composition of Fe-12Cr-5Al, as 5%Al was identified as being the minimum Al content needed for low mass change in Pb-Li at 700°C.[17] Based on the oxide stability experiments, combinations of Y_2O_3 and ZrO_2 or HfO_2 were initially fabricated along with only Y_2O_3. A fourth alloy with Y_2O_3 and TiO_2 also is being processed but has not been extruded yet.

Experimental Procedure

Three experimental ODS FeCrAl ferritic alloys were produced by mechanical alloying (MA). Powder of specified composition Fe-12.1wt.%Cr-5.0Al and particle size range ~45-150 µm was prepared by Ar gas atomization by ATI Metal Powders. The FeCrAl powder was blended with Y_2O_3 powder (17-31 nm crystallite size, produced by Nanophase, Inc.) and batches included ZrO_2 and HfO_2 powders (<100 nm diameter from American Elements). Three 1 kg batches of powder were prepared for ball milling with the following oxide additions: (1) $0.3Y_2O_3$, (2) $0.3Y_2O_3 + 0.4ZrO_2$ and (3) $0.3Y_2O_3 + 0.22HfO_2$. Each batch was ball milled for 40 h in Ar gas atmosphere using the Zoz CM08 Simoloyer. After ball milling, the powders were placed in mild steel cans, degassed at 300ºC under vacuum and sealed. The cans were equilibrated at 950ºC for 1 h and then extruded through a rectangular shaped die. Table 1 shows the as-extruded compositions of each alloy. The alloys with additional ZrO_2 and HfO_2 oxide additions showed higher O contents and the Cr and Al contents were lower than the starting powder. Other typical impurities were Co, Cu, Ni and Mn at the 0.01-0.02% level and the C and N pickups from the milling process were acceptable. Tensile tests were performed using SS-3 type tensile specimens fabricated with the gage section (7.62 mm long and 0.762 mm thick) parallel to the extrusion axis of the ODS FeCrAl heats. The tensile tests were conducted in an MTS hydraulic frame at temperatures ranging from 25ºC-800ºC and a strain rate of 10^{-3} s^{-1}. Polished metallographic specimens were examined with a JEOL model 6500 Field Emission Gun (FEG) Scanning Electron Microscope (SEM) employing X-ray Energy Dispersive Spectroscopy (XEDS). The average grain size was obtained by the line intercept method in terms of the 95-percent confidence interval around the mean. Specimens for Transmission Electron Microscope (TEM) analysis were prepared by Focused Ion Beam (FIB, Hitachi model NB500) using the in-situ lift-out method from the polished metallographic samples of the extruded ODS FeCrAl heats. A Philips model CM200 FEG-TEM/STEM (Scanning TEM) with XEDS and EELS (Electron Energy Loss Spectroscopy) was used for analysis. Bright-Field (BF) and High Angle Annular Dark Field (HAADF) STEM and Energy Filtered TEM (EFTEM) imaging methods were used in the microstructural investigations.

Results and Discussion

The general microstructural features of the ODS FeCrAl heats observed by BF STEM are shown in Figure 1. In the micrographs, the extrusion direction runs horizontally from left to right. The results showed variations in grain size for the three heats (Table 2); the largest grain size was observed with only Y_2O_3 (Figure 1a) and the smallest grain size was observed for $Y_2O_3 + ZrO_2$ (Figure 1b) with that of $Y_2O_3 + HfO_2$ (Figure 1c) in between. The grain size was measured parallel and normal to the extrusion axis to determine the grain aspect ratio (GAR), which is shown in Table 2. The results showed no significant elongation of the grains parallel to the extrusion direction of the heats since the GAR values were <2 for the three heats.

Particles showing dark contrast in BF STEM images were observed in each of the three heats, but a higher number density of these particles was observed in the alloy with $Y_2O_3 + HfO_2$ (Figure 1c). Higher

Table 1. Alloy chemical compositions (mass% or ppmw) by inductively coupled plasma analysis and combustion analysis.

Material	Fe%	Cr%	Al%	Y%	O	C	N	S	Other
Powder	82.8	12.1	5.0	<	64	31	11	<3	0.004Si
125Y	83.3	11.4	4.8	0.19	842	380	455	20	0.05W, 0.02Si, 0.01Ti
125YZ	82.8	11.5	4.9	0.18	1920	250	161	10	0.30Zr, 0.01Hf, 0.01Si
125YH	82.3	11.7	4.8	0.17	2280	220	110	10	0.68Hf, 0.01Zr, 0.01Si
PM2000	74.1	19.1	5.5	0.39	2480	14	86	8	0.48Ti, 0.02Si

< indicates below the detectability limit of <0.01%

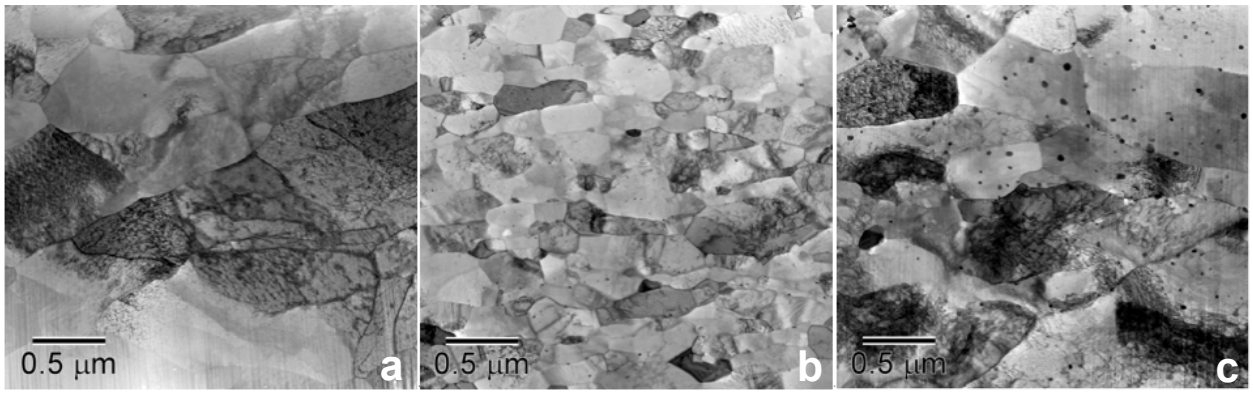

Figure 1. BF STEM micrographs showing the grain size and structure of the extruded ODS FeCrAl heats; (a) with Y_2O_3, (b) Y_2O_3 + ZrO_2 and (c) Y_2O_3 + HfO_2. The extrusion axis lies horizontal from left to right.

magnification images of the oxide particle dispersions in each heat are shown in Figure 2. The microstructural analysis revealed bimodal particle sizes in the alloys with Y_2O_3 and Y_2O_3 + ZrO_2 and a trimodal particle size with Y_2O_3 + HfO_2 based on differences in size and phase, i.e. image contrast and XEDS. The average particle size (d) determined from the bimodal and trimodal size distributions of the ODS FeCrAl heats are shown in Table 3. In general, the oxide particles observed in the bimodal size distributions with Y_2O_3 and Y_2O_3 + ZrO_2 showed dark contrast relative to the surrounding matrix in HAADF STEM images suggesting that they are an oxide phase. The oxygen-enriched nanoclusters observed in the advanced ODS 14YWT ferritic alloy have also been shown to exhibit darker contrast than the surrounding matrix when imaged by HAADF (commonly known as Z or atomic number contrast), since the intensity scales with Z^2.[20] The smaller particles (d ~ 2.5 nm with only Y_2O_3 and d ~ 2.9 nm with Y_2O_3 + ZrO_2) were present within grains and showed the highest number densities. A lower number density of larger particles (d ~ 7 with only Y_2O_3 and d ~ 9 nm with Y_2O_3 + ZrO_2) were mostly associated near grain boundaries in these heats. In the trimodal size distribution with Y_2O_3 + HfO_2, only the smallest particles (d ~ 3.2 nm) showed dark contrast in HAADF STEM images as shown in Figure 3. Particles in the intermediate size range (d ~ 14.5 nm) showed dark and bright contrast (indicated by arrows) while those in the largest size range (d ~ 28 nm) showed bright contrast relative to the surrounding matrix, Table 3. The XEDS analysis of the largest particles showed that they were Hf-rich. The size distributions determined for the different types of particles observed in each heat are shown in Figure 4. In the counting assessment, an equal number of particles were measured in each population and are distinguished in the bar graphs with different colors. It is possible that the particles comprising the bimodal size distributions observed with only Y_2O_3 (Figure 4a) and with Y_2O_3 + ZrO_2 (Figure 4b) are the same phase indicating that the particles experienced different nucleation mechanisms, for example, higher solute diffusion rates near grain boundaries compared to bulk diffusion rates in the grains. For the alloy with Y_2O_3 + HfO_2 (Figure 4c), the scale for particle sizes was increased to show the trimodal size distributions, which accounts for the high frequency value observed for particles below 5 nm in size. The results show three distinct particle size ranges representing the different oxide phases present in this alloy.

Table 2. Measurements of the grain size and grain aspect ratio (GAR) of the ODS FeCrAl ferritic alloys.

Alloy	Grain Size (μm)		GAR
	Parallel to Extrusion Axis	Normal to Extrusion Axis	(Parallel/Normal)
125Y	0.83 ± 0.17	0.56 ± 0.09	1.48
125YZ	0.27 ± 0.06	0.17 ± 0.02	1.59
125YH	0.70 ± 0.16	0.39 ± 0.06	1.79

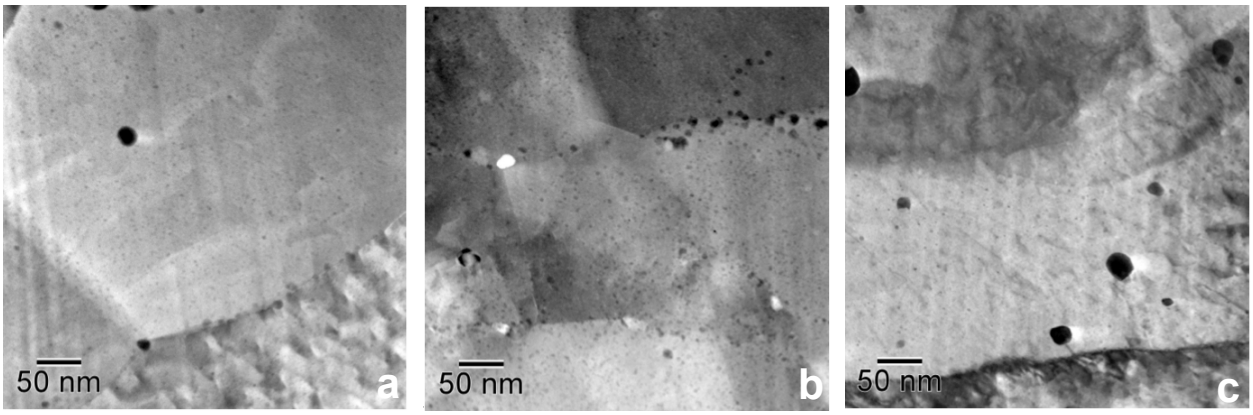

Figure 2. STEM micrographs showing the oxide particle dispersions in the extruded ODS FeCrAl heats; (a) BF STEM with Y_2O_3, (b) HAADF STEM with Y_2O_3 + ZrO_2 and (c) BF STEM with Y_2O_3 + HfO_2.

Table 3. Measurements of the particle size diameters (nm) of the three Fe-12Cr-5Al heats based on the type of particle contrast in the HAADF images.

Alloy	Small dark contrast	Large dark contrast	Dark/bright contrast	Large bright contrast (Hf-rich)
125Y	2.43 ± 0.36	6.87 ± 0.82	–	–
125YZ	2.91 ± 0.32	8.97 ± 0.85	–	–
125YH	3.18 ± 0.51	–	14.58 ± 2.18	27.77 ± 3.49

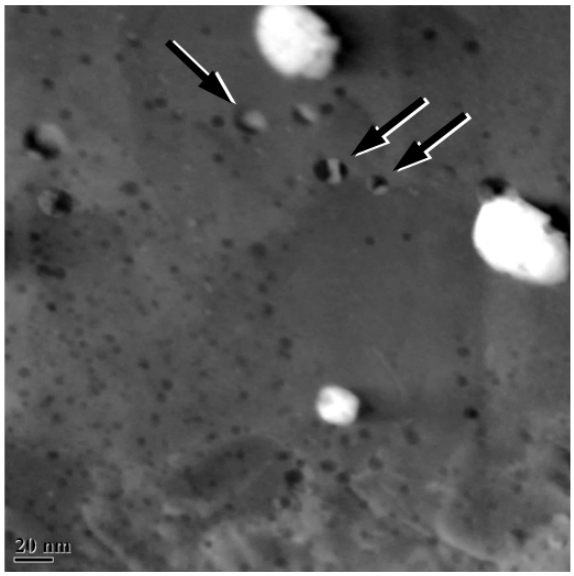

Figure 3. HAADF STEM image of the alloy with Y_2O_3 + HfO_2 showing the contrast characteristics of three different particles; small dark contrast, dark/bright contrast (arrows) and large bright Hf-rich contrast.

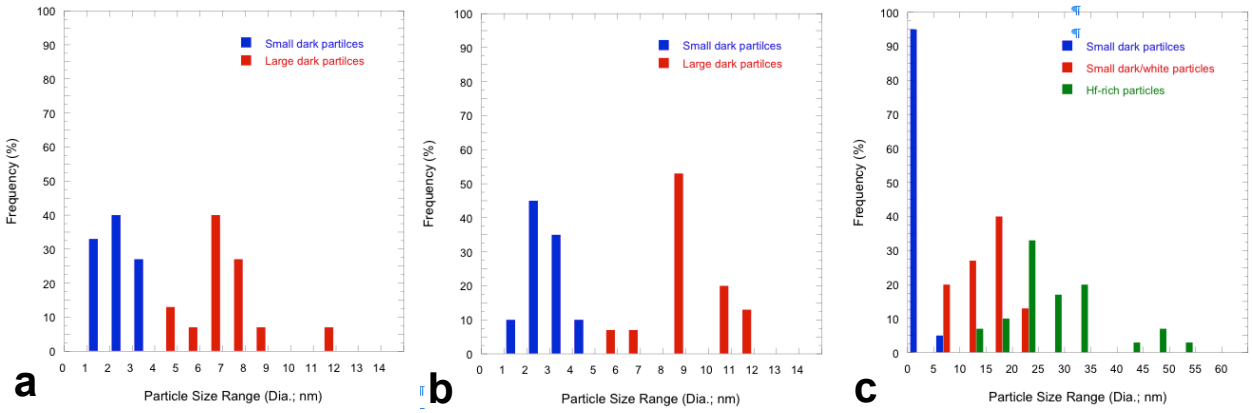

Figure 4. The size distributions measured for the different oxide particles observed in the ODS FeCrAl heats; (a) with Y_2O_3, (b) Y_2O_3 + ZrO_2 and (c) Y_2O_3 + HfO_2.

The results of the tensile testing from 25º-800ºC are shown in Figure 5 and are compared to data for unrecrystallized PM2000 (composition shown in Table 1). The values for yield stress (σ_{ys}) and ultimate tensile strength (σ_{uts}) and their temperature dependence were similar with Y_2O_3 + ZrO_2 and Y_2O_3 + HfO_2 (Figure 5c) and consistently higher than the values with only Y_2O_3, Figure 5a. All of the new alloys were higher than the values for PM2000. At room temperature, the σ_{ys} was >1200 MPa and the σ_{uts} was >1300 MPa for the alloys with greater oxide additions compared to σ_{ys} = 1017 MPa and σ_{uts} = 1235 MPa for the alloy with only Y_2O_3. Both alloys with Y_2O_3 + ZrO_2 and with Y_2O_3 + HfO_2 retained significant levels of strength at 800ºC, with σ_{ys} = 327 and 304 MPa and σ_{uts} = 381 and 334 MPa, respectively. These are considerably higher than the σ_{ys} = 73 MPa and σ_{uts} = 120 MPa measured for PM2000 at 800°C. However, considerably different behavior was observed for the total elongation measurements in these tensile tests, Figure 5b. The elongation for PM2000 was significantly higher than any of the 12Cr-5Al alloys, especially at the higher temperatures. The large difference for PM2000 is likely related to the extrusion conditions and requires further study. Among the new alloys, both the uniform elongation and total elongation were

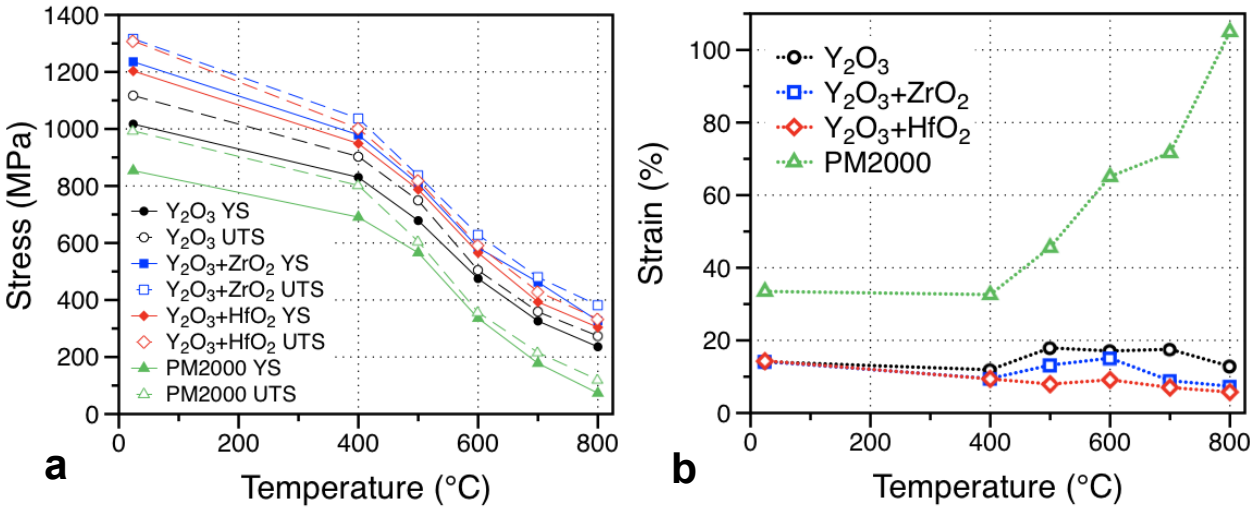

Figure 5. Tensile properties of the ODS FeCrAl heats as a function of test temperature. (a) yield stress and ultimate tensile strength and (b) total elongation.

very similar at room temperature. As the test temperature increased from 25º to 800ºC, the total elongation was consistently highest for the alloy with only Y_2O_3 compared to the other two alloys. The alloy with Y_2O_3 + ZrO_2 had slightly higher ductility at 500° and 600°C. All of the new heats showed reasonable work hardening from 25º to 800ºC, except for the alloy with only Y_2O_3, which showed very little work hardening capacity at 800ºC.

References

[1] M. Abdou, D. Sze, C. Wong, M. Sawan, A. Ying, N. B. Morley and S. Malang, Fus. Sci. Tech., 47 (2005) 475.

[2] O. K. Chopra, D. L. Smith, P. F. Tortorelli, J. H. DeVan and D. K. Sze, Fusion Technol., 8 (1985) 1956.

[3] J. Konys, W. Krauss, J. Novotny, H. Steiner, Z. Voss and O. Wedemeyer, J. Nucl. Mater. 386-88 (2009) 678.

[4] S. Ukai and M. Fujiwara, J. Nucl. Mater. 307 (2002) 749.

[5] G. R. Romanowski, L. L. Snead, R. L. Klueh, D. T. Hoelzer, J. Nucl. Mater., 283-287 (2000) 642.

[6] R. L. Klueh, J. P Shingledecker, R. W. Swindeman, D. T. Hoelzer, J. Nucl. Mater. 341 (2005) 103.

[7] D. A. McClintock, M. A. Sokolov, D. T. Hoelzer and R. K. Nanstad, J. Nucl. Mater., 392 (2009) 353.

[8] T. Furukawa, G. Müller, G. Schumacher, A. Weisenburger, A. Heinzel and K. Aoto, J. Nucl. Mater. 335 (2004), 189.

[9] P. Hosemann, H.T. Thau, A.L. Johnson, S.A. Maloy and N. Li, J. Nucl. Mater. 373 (2008) 246.

[10] C. Schroer, J. Konys, T. Furukawa and K. Aoto, J. Nucl. Mater. 398 (2010) 109.

[11] A. Weisenburger, K. Aoto, G. Müller, A. Heinzel, G. Schumacher and T. Furukawa, J. Nucl. Mater. 358 (2006) 69.

[12] B. A. Pint, L. R. Walker and K. A. Unocic, Mater. High Temp. 29 (2012) 129.

[13] J. D. Whittenberger, Met. Trans. 9A (1978) 101.

[14] J. Lim, H.O. Nam, I.S. Hwang and J.H. Kim, J. Nucl. Mater. 407, (2010), 205.

[15] A. Kimura, et al., J. Nucl. Mater. 417, (2011), 176.

[16] S. Takaya, et al., J. Nucl. Mater. 428, (2012), 125

[17] B. A. Pint, D. T. Hoelzer, D. Shin, J. O. Kiggans, Jr., K. A. Unocic, DOE/ER-0313/53 (2012) 10.

[18] B. A. Pint, D. T. Hoelzer and K. A. Unocic, DOE/ER-0313/54 (2013) 27.

[19] C. Capdevila, M.K. Miller, K.F. Russell, J. Chao, J.L. González-Carrasco, Mater. Science and Engineering A, 490, (2008), 277.

[20] M.C. Brandes, L. Kovarik, M.K. Miller and M.J. Mills, Journal of Materials Science, 47, (2012), 3913.